Research paper

Identification of radical reactions and products for aqueous hydroxylamine nitrate (HAN) solution based on ab initio calculations

Yu-ichiro Izato*† and Atsumi Miyake**

*Graduate School of Environment and Information Sciences, Yokohama National University, 79–7 Tokiwadai, Hodogaya–ku, Yokohama–shi, Kanagawa, 240–8501 JAPAN
Phone: +81–45–339–3981
†Corresponding author: izato–yuichiro–hk@ynu.jp

**Institute of Advanced Sciences, Yokohama National University, 79–7 Tokiwadai, Hodogaya–ku, Yokohama–shi, Kanagawa, 240–8501 JAPAN

Received: June 16, 2017 Accepted: April 20, 2018

Abstract

A mechanism for the radical reactions of hydroxylamine nitrate (HAN) in the aqueous phase was identified and investigated. Optimized structures for the reactants, products and transition states were obtained at the ωB97X-D/6-311++G(d,p)/SCRF=(solvent=water) level of theory and the total electron energies of such structures were calculated at the CBS-QB3 level of theory. The H· abstraction reactions, $NH_2OH + OH\cdot$, $NH_2OH + NO_2\cdot$, $NH_2O\cdot$ (or HNOH·) + OH·, $NH_2O\cdot$ (or HNOH·) + $NO_2\cdot$, HNO + OH·, HNO + $NO_2\cdot$, and other reactions including decomposition of HONO and HNO were investigated. HAN ($[NH_2OH][HNO_3]$) has a high reactivity and ignitability compared to ammonium nitrate ($[NH_3][HNO_3]$). H· abstraction from NH_2OH has a considerably lower barrier than is the one from NH_3. The difference in reactivity of NH_3 and NH_2OH is the source of the difference in thermal stability of ammonium nitrate and HAN. The initial reaction that triggers this mechanism has the highest energy barrier (205.0 kJ mol^{-1}) of all the reactions investigated in this work. Thus, we conclude that the homolytic cleavage of HNO_3 is the rate-determining step for the decomposition of aqueous HAN solution.

Keywords: hydroxylamine nitrate, aqueous phase reaction, reaction mechanism, density functional theory

1. Introduction

Hydrazine and its derivatives are currently used as liquid monopropellants in various spacecraft. However, the toxicity and high volatility of hydrazine and its derivatives make handling difficult and also increase manufacturing costs. Hydroxylamine nitrate (HAN)-based liquid propellant such as SHP163, is one of the most promising candidates as a replacement for commonly used hypergolic propellants such as hydrazine[1)–3)]. For this reason, there have been many experimental and theoretical studies regarding the combustion behavior of HAN-based propellants[4)–11)]. Previous studies have shown that some HAN solutions exhibit extremely high burning rates, and this behavior has limited the potential applications of such propellants[3)–6)], since elevated burning rates can lead to serious accidents[12)–14)]. Therefore, the safe use of HAN-based propellants will require advanced combustion control techniques and an appropriate understanding of the combustion behavior of this compound.

A detailed chemical reaction model is helpful when investigating rapid transient phenomena such as ignition and extinction. Khare et al.[15)] studied the ignition behavior of HAN/water solutions and developed a theoretical model incorporating earlier gas phase[16),17)] and condensed phase reaction models, such as the electrolysis of ionic liquids and the Lee and Litzinger models[18)]. Khare et al.[15)] calculated ignition delays using this same model and discussed the adequacy of electrolytically induced ignition systems for HAN-based propellants. Lee and Litzinger[18)]

developed a reduced reaction model consisting of eight reactions based on previously proposed reaction mechanisms[19),20)], and calculated reaction rates by simulating the experimental decomposition process and applying an inverse analysis technique.

Ab initio computations are useful to determine reactions that should be excluded from a mechanism based on thermodynamic arguments. Our previous theoretical study investigated the initial decomposition and HONO catalytic decomposition of aqueous HAN solutions as represented by reactions; $NH_2OH + HNO_3 \rightleftarrows HONO + HNO + H_2O$ and $NH_2OH + HONO \rightleftarrows N_2O + 2H_2O$[21)]. In the initial decomposition, mechanisms for the charge neutral-neutral bimolecular reactions ($NH_2OH + HNO_3 \rightarrow HNO + HONO + H_2O$ and $NH_3O + HNO_3 \rightarrow HNO + HONO + H_2O$), ion-neutral bimolecular reaction ($NH_3OH^+ + HNO_3 \rightarrow HNO + HONO + H_2O + H^+$) and HNO_3 self-decomposition ($HNO_3 + HNO_3 \rightarrow N_2O_5 + H_2O$) were found. The maximum energy barriers (total electron energy) for each of these reactions were respectively calculated as 124.8, 88.7, 91.7 and 89.8 kJ mol^{-1}. Each of these reaction schemes appears to be thermodynamically viable and all yield the same products. The overall initial decomposition reaction can be summarized using a single equation: HAN → HONO + HNO + H_2O. The primary scheme will depend on the concentrations of the various species in the reaction solution. HAN dissociates to form ion pairs in water, with NH_3OH^+ and NO_3^- being the major species. Therefore, we conclude that the $NH_3OH^+ + HNO_3$ reaction mechanism is dominant during the initial HAN decomposition in aqueous solution.

We also developed six HAN/HONO catalytic decomposition pathways, with each of these schemes providing the same overall reaction: $NH_2OH + HONO \rightarrow N_2O + 2H_2O$[21)]. These schemes can be divided according to combinations of oxidizers (HONO, *trans*-$ONONO_2$ (*t*-$ONONO_2$) or N_2O_3) and reductants (NH_2OH or NH_3OH^+). In the HONO oxidizing scheme, HONO directly attacks NH_2OH or NH_3OH^+ to yield N_2O and H_2O (or H_3O^+) ($\Delta E_0^{\ddagger}$ = 171.2 or 74.9 kJ mol^{-1}). In the *t*-$ONONO_2$ scheme, HONO reacts with HNO_3 to give *t*-$ONONO_2$ ($\Delta E_0^{\ddagger}$ = 11.4 kJ mol^{-1}) and the *t*-$ONONO_2$ oxidizes NH_2OH or NH_3OH^+ ($\Delta E_0^{\ddagger}$ = −44.8 or 22.6 kJ mol^{-1}). In the N_2O_3 mechanism, two HONO molecules decompose to yield N_2O_3 ($\Delta E_0^{\ddagger}$ = 50.4 kJ mol^{-1}) and the N_2O_3 oxidizes NH_2OH or NH_3OH^+ ($\Delta E_0^{\ddagger}$ = −1.7 or 33.9 kJ mol^{-1}). Based on the energy barrier results, the *t*-$ONONO_2$ oxidizing scheme is the most plausible.

All possible reaction paths should be included in the detailed reaction model to predict the combustion behavior of HAN-based propellants accurately. Our previous study[22)] did not cover radical reactions initiated by homolytic cleavage of HNO_3. HAN must have a radical reaction in the decomposition path analogous to ammonium nitrate (AN). AN, which has a similar chemical structure ($[NH_4]^+[NO_3]^-$) to HAN ($[NH_3OH]^+[NO_3]^-$), has two reaction paths, ionic and radical[22)−24)]. As the temperature increases, the ionic decomposition of AN is thought to be overtaken by high temperature radical decomposition, and Brower et al.[25)] suggested a mechanism for the radical reaction of AN at elevated temperatures (> 563 K). Brower et al.[25)] also revealed that the cleavage of HNO_3, $HNO_3 \rightarrow OH\cdot + NO_2\cdot$, was found to trigger the AN radical reaction and the major products were determined to be N_2O and H_2O, generated via NH_2NO_3. In this mechanism, AN initially dissociates into HNO_3 and NH_3, followed by homolytic cleavage of the HO-N bond in HNO_3. Following this cleavage, a fast radical-chain reaction develops and yields large amounts of gaseous N_2, NO and H_2O with large exothermic heat.

The aim of the present study is to gain a better understanding of the radical decomposition path in aqueous HAN solution based on ab initio principles. To this end, we have investigated energetics of reactions by using quantum chemistry computations, which are helpful with regard to determining which reactions to remove from the mechanism based on thermodynamics. If a reaction is found to be highly endothermic, or considerably more endothermic than a competing pathway, then that reaction may be safely omitted from the mechanism.

2. Computational

The geometries of the reactants, products and transition states (TSs) were optimized at the ωB97X-D[26)]/6-311++G(d,p)/SCRF=(solvent=water) level of theory using the Gaussian 09 program package[27)]. Gordon et al.[26)] developed the ωB97X-D method, which includes empirical dispersion forces and is believed to be reliable when applied to systems with weak van der Waals forces. Their group also reported that the ωB97X-D method yields satisfactory accuracy for kinetics and non-covalent interactions[26)]. During computations, TSs were extensively searched for and, if found, an intrinsic reaction coordinate (IRC) calculation was conducted in order to assign reactants and products to the TS.

The energies of corresponding molecules were evaluated at the CBS-QB3[28)]/SCRF=(solvent=water) level of theory, since this is a reasonable time-expense complete basis method. In this study, geometries and frequencies were calculated at the ωB97X-D/6-311++G(d,p) level, the optimized geometries were fixed with no changes allowed, and the energies were calculated using the CBS-QB3 method. CBS-QB3 is understood to represent a cost-effective strategy for obtaining chemically accurate thermochemical calculations.

Solvent effects were included by applying the self-consistent reaction field (SCRF) and polarizable continuum model (PCM) options within the program when investigating the reactions of aqueous HAN solution. We applied the dielectric constant of water (ε = 78.3553).

3. Results and discussion

The important reactions associated with the radical decomposition of aqueous HAN solution, along with their energy barriers and energy changes calculated at the CBS-QB3//ωB97X-D/6-311++G(d,p)/SCRF=(solvent=water) level of theory, are provided in Table 1. These reactions are discussed in detail in the following sections. In the case of each reaction addressed in this paper, the total energy

change at 0 K (ΔE_0) between the transition state and the reactants ($\Delta E_0^{\ddagger}$) is considered. It should be noted that any prediction of chemical reactions makes use of free energy. However, a method that can provide accurate free energies of aqueous-phase molecules has not yet been established. The contribution of solvent effects obtained using the SCRF is normally added to the electronic energy using standard quantum chemical programs. Other contributions to the enthalpy and entropy are evaluated using the formalism based on statistical mechanics under the ideal-gas model assumption. That might be the cause of significant errors in computing free energy of liquid species. The effect of the nuclear motions of the solutes, which is not included explicitly by the SCRF treatment, also contributes to the thermodynamic properties. Thus, we used the total energy change to discuss a reasonable reaction path in this study.

3.1 Homolytic cleavage of nitric acid: $HNO_3 \rightarrow NO_2\cdot + OH\cdot$

Homolytic cleavage of HNO_3 (R1) starts the radical reaction. We investigated the reaction in a previous study to identify the radical reaction path of ammonium nitrate[22]. The associated energy barrier was calculated to be 205.0 kJ mol^{-1} at the CBS-QB3//ωB97X-D/6-311++G(d, p)/SCRF=(solvent=water) level of theory.

3.2 NH_2OH + radicals

Following R1, the decomposition proceeds via a fast radical-chain reaction. We identified and investigated possible initial chain-propagating reactions as below (R2 and R3).

$$NH_2OH + OH\cdot \rightarrow NH_2O\cdot + H_2O \quad (R2)$$
$$NH_2OH + OH\cdot \rightarrow HNOH\cdot + H_2O \quad (R3)$$

Figure 1 depicts the potential energy profiles and optimized structures for this reaction. Here, the OH· abstracts H· from NH_2OH. There are two methods for H· abstraction. One is a transition from the OH in NH_2OH to yield NH_2O· and the other is from NH_2· to yield HNOH·. The associated energy barriers for these reactions in water were determined to be 10.5 kJ mol^{-1} (R2) and 5.2 kJ mol^{-1} (R3), respectively, at the CBS-QB3//ωB97X-D/6-311++G(d,p)/SCRF=(solvent=water) level of theory. The associated heats of reaction were −191.3 and −145.2 kJ mol^{-1} at the same level of theory. R3 is kinetically

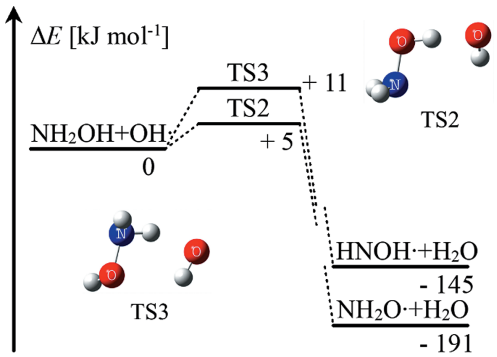

Figure 1 Potential energy profile for the reaction of NH_2OH + OH·, as calculated at the CBS-QB3//ωB97X-D/6-311++G (d, p) /SCRF= (solvent=water) level of theory.

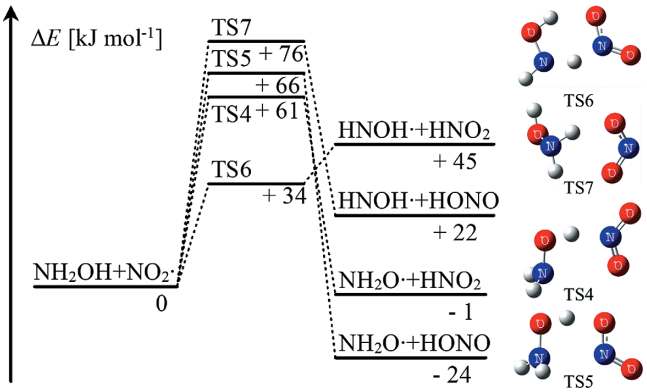

Figure 2 Potential energy profiles for the reactions of NH_2OH + NO_2·, as calculated at the CBS-QB3//ωB97X-D/6-311++G (d, p) /SCRF= (solvent=water) level of theory.

preferable to R2, but R2 is thermally preferable to R3.

This work also identified other initial chain-propagating reaction series following R1, as shown below (R4−R7).

$$NH_2OH + NO_2\cdot \rightarrow NH_2O\cdot + HNO_2 \quad (R4)$$
$$NH_2OH + NO_2\cdot \rightarrow NH_2O\cdot + HONO \quad (R5)$$
$$NH_2OH + NO_2\cdot \rightarrow NHOH\cdot + HNO_2 \quad (R6)$$
$$NH_2OH + NO_2\cdot \rightarrow NHOH\cdot + HONO \quad (R7)$$

Figure 2 shows the potential energy profiles for these four reactions as well as the optimized structures. The H· abstraction from NH_2OH can be divided into four reactions by combination of product species (NH_2O·, HNOH·, HNO_2, and HONO). The associated energy barriers of R4−R7 were calculated to be 66.4, 61.2, 34.3, and 76.3 kJ mol^{-1}, and the associated heats of reaction calculated to be −1.2, −23.8, 44.9, and 22.3, respectively. R4 and R5 are exothermic reactions, but R6 and R7 are endothermic reactions because HNOH· is an unstable radical compared to NH_2O·. The energy barrier and heat of reaction indicated that R6 is kinetically preferable, but R5 is thermally preferable.

We previously calculated the energy barrier for the analogous H· abstraction reactions between NO_2· and NH_3 in the reaction mechanism of AN decomposition at the same level of theory[22]. The energy barrier and heat of reaction were determined to be 144.7 ($NH_3+NO_2\cdot \rightleftharpoons NH_2+HNO_2$) and 116.6 kJ mol^{-1} ($NH_3+NO_2\cdot \rightleftharpoons NH_2+HONO$), respectively. Because these barriers are too high compared to other possible reactions in AN decomposition, we concluded that these reactions are not dominant in AN decomposition. In contrast, H· abstractions from NH_2OH have much more reasonable barriers than ones from NH_3. The difference in reactivity of NH_3 and NH_2OH seems to be the cause for the difference in thermal stability of AN and HAN.

3.3 $NH_2O\cdot$ + radicals and $HNOH\cdot$ + radicals

This work examined the radical-quenching reaction between NH_2O·, HNOH· and OH· as follows (R8−R11).

$$NH_2O\cdot + OH\cdot \rightarrow NH_2(O)OH \quad (R8)$$
$$NH_2(O)OH \rightarrow HNO + H_2O \quad (R9)$$
$$HNOH\cdot + OH\cdot \rightarrow HN(OH)_2 \quad (R10)$$
$$HN(OH)_2 \rightarrow HNO + H_2O \quad (R11)$$

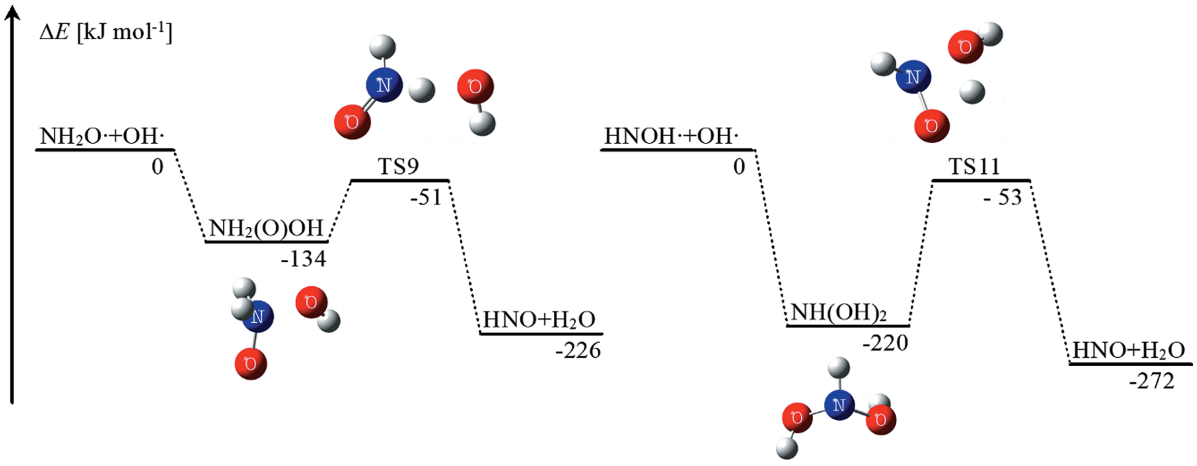

Figure 3 Potential energy profiles for the reactions of $NH_2O\cdot$ + OH· and HNOH· + OH·, as calculated at the CBS-QB3//ωB97X-D/6-311++G (d, p) /SCRF= (solvent=water) level of theory.

The calculation at the CBS-QB3//ωB97X-D/6-311++G(d,p) /SCRF=(solvent=water) level of theory reveals that R8 and R10 does not have a barrier and the radicals binds to produce intermediates, as shown in Figure 3. Then, the intermediates decompose to yield same products, HNO and H_2O, via transition states.

This work also examined other radical-quenching reactions between $NH_2O\cdot$ and $NO_2\cdot$ following R2 (R12−R15).

$$NH_2O\cdot + NO_2\cdot \rightarrow HNO + HONO \quad (R12)$$
$$NH_2O\cdot + NO_2\cdot \rightarrow HNO + HNO_2 \quad (R13)$$
$$NHOH\cdot + NO_2\cdot \rightarrow HNO + HONO \quad (R14)$$
$$NHOH\cdot + NO_2\cdot \rightarrow HNO + HNO_2 \quad (R15)$$

Figure 4 shows the potential energy profile for these four reactions as well as the optimized structures. The H· abstraction from $NH_2O\cdot$ can be divided into two reactions by product species (HNO_2 and HONO). The energy barriers of R12 and R13 were calculated to be 50.4 and 41.3 kJ mol^{-1}, and the associated heats of reaction calculated to be −36.0 and −58.6 kJ mol^{-1}, respectively. R12 yielding HONO is preferable to R13 yielding HNO_2 both kinetically and thermally. The H· abstraction from HNOH· can also be divided into two reactions by product species. The energy barriers of R14 and R15 were calculated to be 44.5 and 101.3 kJ mol^{-1}, and the associated heats of reaction calculated to be −82.1 and −104.7 kJ mol^{-1}, respectively. Because the energy barrier is much higher for R15 than R 14, R15 can be omitted from possible reaction paths.

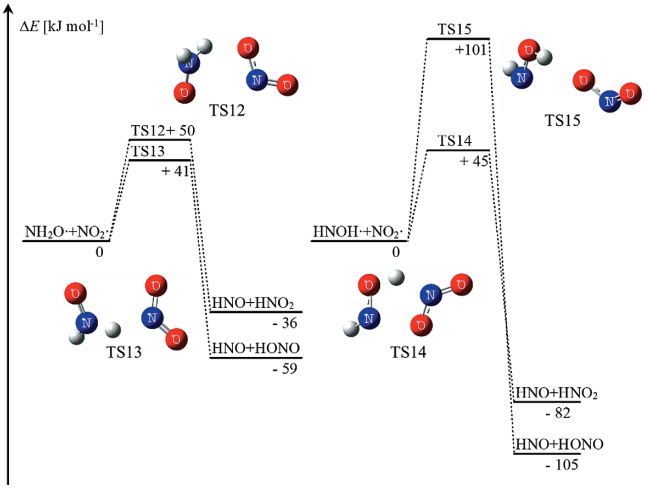

Figure 4 Potential energy profiles for the reactions of $NH_2O\cdot$ + $NO_2\cdot$ and HNOH· + $NO_2\cdot$, as calculated at the CBS-QB3//ωB97X-D/6-311++G (d, p) /SCRF= (solvent= water) level of theory.

3.4 Decomposition of nitroxyl (HNO)

This work investigated decomposition of nitroxyl (HNO). First, H· subtraction from HNO by OH· and $NO_2\cdot$ was examined.

$$HNO + OH\cdot \rightarrow NO\cdot + H_2O \quad (R16)$$
$$HNO + NO_2\cdot \rightarrow NO\cdot + HONO \quad (R17)$$
$$HNO + NO_2\cdot \rightarrow NO\cdot + HNO_2 \quad (R18)$$

Figure 5 depicts the potential energy profile and optimized structures for this reaction. Here, OH· and $NO_2\cdot$ abstract H· from HNO. The associated energy barriers for these reactions in water were determined to be 7.9, 17.5 kJ mol^{-1}, and 42.2 kJ mol^{-1}, respectively, at the CBS-QB3//ωB 97X-D/6-311++G(d,p)/SCRF=(solvent=water) level of theory.

HNO decomposes via the dimer of hyponitrous acid[29),30)]. Thus, this work also investigated dimerization and decomposition of HNO as follows.

$$HNO + HNO \rightarrow HN(O)NHO \quad (R19)$$
$$HN(O)NHO\ (+ H_2O) \rightarrow N(O)NHOH\ (+ H_2O) \quad (R20, R21)$$
$$N(O)NHOH\ (+ H_2O) \rightarrow N_2O + H_2O\ (+ H_2O) \quad (R22, R23)$$

Figure 6 presents the potential energy profiles and optimized structures for the decomposition of the intermediate species HN(O)NHO and N(O)NHOH. HNO first dimerizes to yield hyponitrous acid (HN(O)NHO), then HN(O)NHO subsequently decomposes to N_2O and H_2O via intramolecular proton transition with exothermic reaction. Here, the presence of water assists this process (R21 and R23). Reactions in which water molecules serve as proton-transfer agents are common. The transition states proposed in the absence of explicit solvent molecules typically involve highly strained rings since these are necessary to transfer the proton from one position in the molecule to another. The result is usually a high energetic barrier to the reaction. The inclusion of

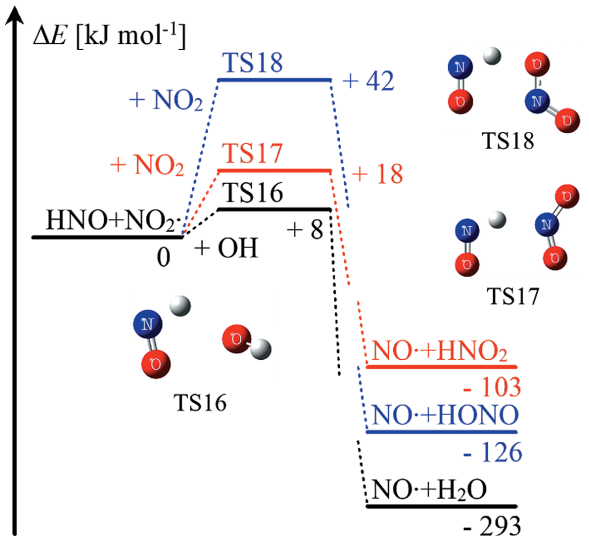

Figure 5 Potential energy profiles for the reactions of HNO + OH· and NO_2·, as calculated at the CBS-QB3//ωB97X-D/6-311++G (d, p) /SCRF= (solvent=water) level of theory.

solvent molecules allows the ring structure (TS21 and TS 23) to be larger and less strained, reducing the transition state energy compared to a small, cyclic transition state structure. Here, one or more water molecules simultaneously accept a hydrogen atom at a lone pair site and give up one of the original hydrogen atoms to another molecule. In the R23, two transition states (TS23 and TS23 -2) were found as shown in Figure 6, and the second barrier associated with N_2O unbending can be negligible due to low barrier (8.4 kJ mol^{-1}).

3.6 Other reactions including HONO and HNO_2

This work revealed that HNO_2 isomerizes to HONO as follows.

$$HNO_2 + HNO_2 \rightarrow HONO + HONO \quad \text{(R25)}$$

Table 1 shows HONO is thermally stable and the barrier is determined to be 38 kJ mol^{-1}. This calculation also shows that HNO_2 produced by H· abstraction is promptly isomerized to HONO.

HONO can then cleave homolytically, analogous to HNO_3 as follows.

$$HONO \rightarrow OH· + NO· \quad \text{(R24)}$$

There is no significant TS from the dissociation of HONO to form OH· and NO·. The energy change of the reaction was determined to be 201.3 kJ mol^{-1} at the CBS-QB3//ωB 97X-D/6-311++G(d,p)/SCRF=(solvent=water) level of theory. This barrier is as large as that for HNO_3 homolysis, which has a much higher barrier than other reactions including HONO, for example, HNO_3 + HONO→ *t*-$ONONO_2$ + H_2O (11.4 kJ mol^{-1})[21]. Thus, the homolytic cleavage of HONO can be omitted from any reasonable reaction path.

3.9 A reaction scheme of radical decomposition of aqueous HAN solution

Figure 7 depicts the radical reaction scheme generated from this work. In this mechanism, HAN initially dissociates to HNO_3 and NH_2OH. The cleavage of HNO_3 triggers the radical decomposition. OH· and NO_2· released from HNO_3 attack NH_2OH to yield NH_2O· (or HNOH),

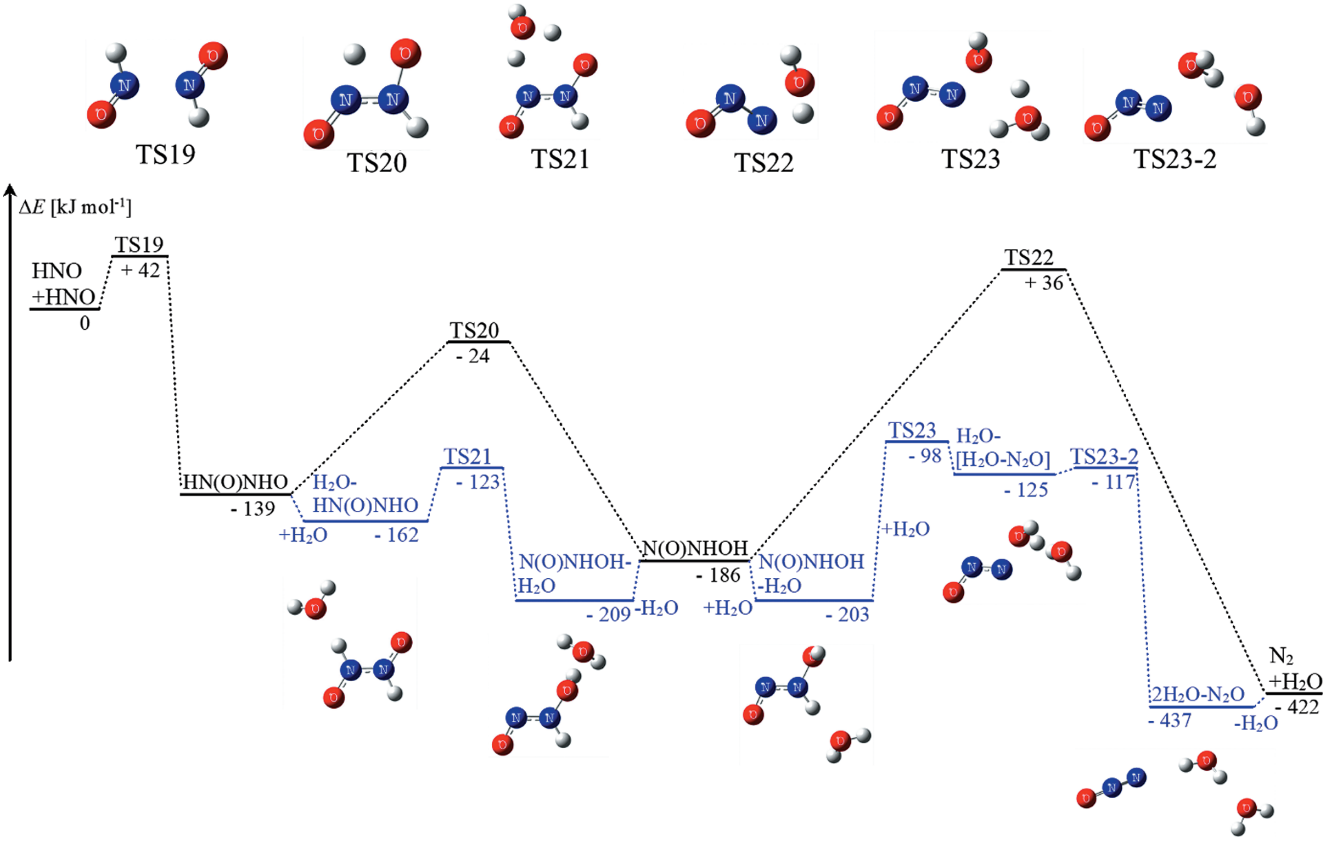

Figure 6 Potential energy profiles for the decomposition of intermediate HNO, as calculated at the CBS-QB3//ωB97X-D/6-311++G (d, p) /SCRF= (solvent=water) level of theory.

Table 1 Important reactions associated with the radical decomposition of HAN in the aqueous phase.

No.	Reaction	CBS-QB3//ωB97X-D/6−311++G(d,p)/SCRF=(solvent=water)	
		ΔE_0 a)	$\Delta_r E_0$ b)
R1	$HNO_3 \rightleftharpoons OH\cdot + NO_2\cdot$	−	205.0
R2	$NH_2OH + OH\cdot \rightleftharpoons NH_2O\cdot + H_2O$ (TS2)	10.5	−191.3
R3	$NH_2OH + OH\cdot \rightleftharpoons NHOH\cdot + H_2O$ (TS3)	5.2	−145.2
R4	$NH_2OH + NO_2\cdot \rightleftharpoons NH_2O\cdot + HNO_2$ (TS4)	66.4	−1.2
R5	$NH_2OH + NO_2\cdot \rightleftharpoons NH_2O\cdot + HONO$ (TS5)	61.2	−23.8
R6	$NH_2OH + NO_2\cdot \rightleftharpoons NHOH\cdot + HNO_2$ (TS6)	34.3	44.9
R7	$NH_2OH + NO_2\cdot \rightleftharpoons NHOH\cdot + HONO$ (TS7)	76.3	22.3
R8	$NH_2O\cdot + OH\cdot \rightleftharpoons NH_2(O)OH$	0	−134.4
R9	$NH_2(O)OH \rightleftharpoons HNO + H_2O$ (TS9)	83.7	−91.6
R10	$NHOH\cdot + OH\cdot \rightleftharpoons HN(OH)_2$	0	−219.8
R11	$HN(OH)_2 \rightleftharpoons HNO + H_2O$ (TS11)	167.3	−52.4
R12	$NH_2O\cdot + NO_2\cdot \rightleftharpoons HNO + HNO_2$ (TS12)	50.4	−36.0
R13	$NH_2O\cdot + NO_2\cdot \rightleftharpoons HNO + HONO$ (TS13)	41.3	−58.6
R14	$NHOH\cdot + NO_2\cdot \rightleftharpoons HNO + HNO_2$ (TS14)	44.5	−82.1
R15	$NHOH\cdot + NO_2\cdot \rightleftharpoons HNO + HONO$ (TS15)	101.3	−104.7
R16	$HNO + OH\cdot \rightleftharpoons HNO + H_2O$ (TS16)	7.9	−293.1
R17	$HNO + NO_2\cdot \rightleftharpoons HNO + HNO_2$ (TS17)	17.5	−103.0
R18	$HNO + NO_2\cdot \rightleftharpoons HNO + HONO$ (TS18)	42.2	−125.6
R19	$HNO + HNO \rightleftharpoons HN(O)NHO$ (TS19)	42.0	−138.5
R20	$HN(O)NHO \rightleftharpoons N(O)NHOH$ (TS20)	115.9	−47.0
R21	$HN(O)NHO + H_2O \rightleftharpoons N(O)NHOH + H_2O$ (TS21)	15.6	−47.0
R22	$N(O)NHOH \rightleftharpoons N_2O + H_2O$ (TS22)	222.3	−236.0
R23	$N(O)NHOH + H_2O \rightleftharpoons N_2O + 2H_2O$ (TS23, TS23−2)	95.8	−236.0
R24	$HONO \rightleftharpoons OH\cdot + NO\cdot$	−	201.3
R25	$HONO + HONO \rightleftharpoons HNO_2 + HNO_2$ (TS25)	38.3	−45.2

a) energy barrier in the forward direction [kJ mol^{-1}]

b) total energy change of reaction [kJ mol^{-1}]

HNO_2 (or HONO), and H_2O, after which a major part of the $NH_2O\cdot$ (and HNOH·) reacts with radicals ($NO_2\cdot$ or OH·) to give HNO, which then decomposes to N_2O and two H_2O molecules via dimerization or reacts with radicals to form NO·. $NO_2\cdot$ abstracts H· from NH_2OH, NH_2O, HNOH, or HNO to form HONO or HNO_2. HNO_2 can promptly isomerize to HONO.

After producing HONO, a HONO catalytic reaction also occurs. The energy barrier for the rate determining step in the HONO catalytic reaction HNO_3 + HONO→ *t*-$ONONO_2$ + H_2O is 11.4 kJ mol^{-1} of total electron energy at the CBS-QB3//ωB97X-D/6-311++G(d,p)/SCRF=(solvent=water) level of theory[21]. The energy barrier is much less in the HONO catalytic reaction than in the homolytic cleavage of HNO_3 (205.0 kJ mol^{-1}) and HONO (201.3 kJ mol^{-1}). *t*-$ONONO_2$ promptly reacts with NH_2OH with no energy barrier and the reaction regenerates HNO_3 in an exothermic reaction. Therefore, we conclude that the radical reaction proceeds with the HONO catalytic mechanism after producing HONO. At high temperature, which provides sufficient energy to the HAN solution and allows the unimolecular reaction to take advantage of entropic contributions, mass transfer (diffusion) limitations, and dilution effects, the radical decomposition initiated by the unimolecular reaction might overtake the catalytic decomposition initiated by the bimolecular reaction. An understanding of the transition to radical reactions is important when assessing the possibility of HAN explosions in response to thermal inputs such as irregular combustion in a thruster. Further detailed chemical reaction simulations are needed in the future.

4. Conclusions

The radical reaction pathway for aqueous HAN solution was investigated based on quantum chemical calculations performed at the ωB97X-D/6-311++G(d,p)/SCRF=(solvent=water) and CBS-QB3//ωB97X-D/6-311++G(d,p)/SCRF=(solvent=water) levels of theory. The cleavage of HNO_3, $HNO_3 \rightarrow OH\cdot + NO_2\cdot$, was found to trigger the radical reaction. OH· and $NO_2\cdot$ promptly abstract H· from NH_2OH to yield $NH_2O\cdot$ (or HNOH·), H_2O and HONO ($\rightleftharpoons HNO_2$). The trigger reaction (R1) has the highest energy barrier (205.0 kJ mol^{-1}) in all the reactions investigated in this work. The energy barrier is much large for the homolysis cleavage of HNO_3 than the ionic reaction reported in the previous study[21]. Although the radical reaction does not seem to play an important role in the initial progress of aqueous HAN solutions, the radical reaction can be initiated at high temperature, which provides sufficient energy to break the HO-NO_2 bond in HNO_3. Further detailed chemical

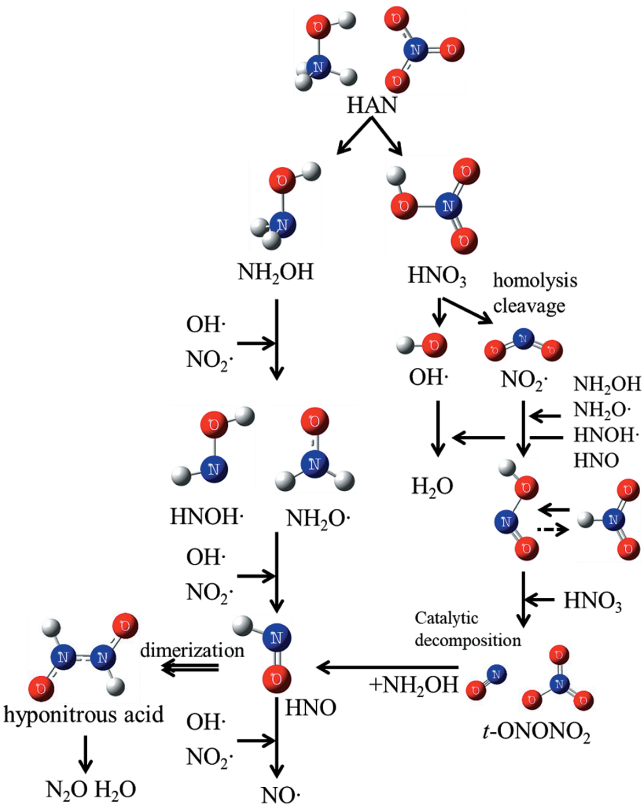

Figure 7 A decomposition scheme for the radical decomposition of HAN.

simulations based on this work (i.e., on radical reactions) and previous work (initial decomposition and HONO catalytic decomposition[21]) will be conducted in the future to clearly elucidate the details on condensed phase decomposition of aqueous HAN solution.

References

1) A. S. Gohardani, J. Stanojev, A. Demairé, K. Anflo, M. Persson, N. Wingborg, and C. Nilsson, Progress in Aerospace Sciences, 71, 128−149 (2014).
2) A. B. Fukuchi, S. Nagase, H. Maruizumi, and M. Ayabe, IHI Engineering Review, 43, 22−28 (2010).
3) T. Katsumi, H. Kodama, T. Matsuo, H. Ogawa, N. Tsuboi, and K. Hori, Combust. Explos. Shock Waves, 45, 442−453 (2009).
4) B. N. Kondrikov, V. Annikov, Y. Egorshev, and L. T. Luca, Combust. Explos. Shock Waves, 36, 135−145 (2000).
5) T. Katsumi, H. Kodama, H. Ogawa, N. Tsuboi, and K. Hori, Sci. Tech. Energetic Materials, 70, 27−32 (2009).
6) T. Katsumi, T. Inoue, J. Nakatsuka, K. Hasegawa, K. Kobayashi, S. Sawai, and K. Hori, Combust, Explos, Shock Waves, 48, 536−543 (2012).
7) Y. Pan, Y. Yu, Y. Zhou, and X. Lu, Propellants Explos. Pyrotech., 37, 439−444 (2012).
8) H. Lee and T. A. Litzinger, Combust. Flame, 127, 2205−2222 (2001).
9) L. Courthéoux, D. Amariei, S. Rossignol, and C. Kappenstein, Applied Catalysis B: Environmental, 62, 217−225 (2006).
10) R. Amrousse, T. Katsumi, A. Bachar, R. Brahmi, M. Bensitel, and K. Hori, Reac Kinet Mech Cat, 111, 71−88 (2013).
11) Y. P. Chang and K. K. Kuo, Assessment of Combustion Characteristics and Mechanisms of a HAN−Based Liquid Monopropellant, Proc. AIAA/ASME/SAE/ASEE Joint Propulsion Conf. and Exibit (AIAA Paper 2001−3272), Salt Lake City, USA (2001).
12) D. G. Harlow, R. E. Felt, S. Agnew, G. S. Barney, J. M. McKibben, R. Garber, and M. Lewis, Technical Report on Hydroxylamine Nitrate, U. S. Department of Energy (1998).
13) C. Wei, W. J. Rogers, and M. S. Mannan, J. Hazz. Matteril, 130, 163−168 (2006).
14) L. Liu, C. Wei, Y. Guo, W. J. Rogers, and M. S. Mannan, J. Hazz. Materil., 162, 1217−1222 (2009).
15) P. Khare, V. Yang, H. Meng, G. A. Risha, and R. A. Yetter, Combust. Sci. Technol, 187, 1065−1078 (2015).
16) P. Khare, "Decomposition and ignition of HAN−based monopropellants by electrolysis". M.S. thesis, Pennsylvania State University (2009).
17) P. Thakre, Y. Duan, and V. Yang, Combust. Flame, 161, 347−362 (2014).
18) H. Lee and T. A. Litzinger, Combust. Flame, 135, 151−169 (2003).
19) J. C. Oxley and K. R. Brower, Thermal Decomposition of Hydroxylamine Nitrate, Proc. SPIE 0872, Propulsion, 63, (1988).
20) N. Klein, Ignition and combustion of the HAN−based liquid propellants. Proc. 27 th JANNAF Combustion Subcommittee Meeting, vol 1. CPIA Publication, 443−450, Cheyenne, USA (1990).
21) Y. Izato, M. Koshi, and A. Miyake. Cent. Eur. J. Energ. Mater., 14, 888−916 (2017).
22) Y. Izato and A. Miyake, Sci. Tech. Energetic Materials, 78, 143−149 (2017).
23) Y. Izato, M. Koshi, and A. Miyake, Int. J. Chem. Kinet., 49, 83−89 (2017).
24) J. C. Oxley, J. L. Smith, and W. Wang, J. Phys. Chem., 98, 3901−3907 (1994).
25) K. R. Brower, J. C. Oxley, and M. P. Tewari, J. Phys. Chem., 93, 4029−4033 (1989).
26) J. D. Chai and M. Head−Gordon, Phys. Chem. Chem. Phys., 10, 6615−6620 (2008).
27) M. J. Frisch, G. W. Trucks, H. B. Schlegel, G. E. Scuseria, M. A. Robb, J. R. Cheeseman, G. Scalmani, V. Barone, B. Mennucci, G. A. Petersson, H. Nakatsuji, M. Caricato, X. Li, H. P. Hratchian, A. F. Izmaylov, J. Bloino, G. Zheng, J. L. Sonnenberg, M. Hada, M. Ehara, K. Toyota, R. Fukuda, J. Hasegawa, M. Ishida, T. Nakajima, Y. Honda, O. Kitao, H. Nakai, T. Vreven, J. A. Montgomery, J. E. Peralta, F. Ogliaro, M. Bearpark, J. J. Heyd, E. Brothers, K. N. Kudin, V. N. Staroverov, T. Keith, R. Kobayashi, J. Normand, K. Raghavachari, A. Rendell, J. C. Burant, S. S. Iyengar, J. Tomasi, M. Cossi, N. Rega, J. M. Millam, M. Klene, J. E. Knox, J. B. Cross, V. Bakken, C. Adamo, J. Jaramillo, R. Gomperts, R. E. Stratmann, O. Yazyev, A. J. Austin, R. Cammi, C. Pomelli, J. W. Ochterski, R. L. Martin, K. Morokuma, V. G. Zakrzewski, G. A. Voth, P. Salvador, J. J. Dannenberg, S. Dapprich, A. D. Daniels, O. Farkas, J. B. Foresman, J. V. Ortiz, J. Cioslowski, and D. J. Fox, Gaussian 09, Revision D.01, Gaussian, Inc., Wallingford CT (2010).
28) J. A. Montgomery, M. J. Frisch, J. W. Ochterski, and G. A. Petersson, J. Chem. Phys., 110, 2822−2827 (1999).
29) K. M. Miranda, Coordin. Chem. Rev., 249, 433−455 (2005).
30) K. Ruud, T. Helgaker, and E. Uggerud, J. Mol. Struc. (Theochem), 393, 59−71 (1997).